

Incorporating the effect of approach slab to the dynamic response of simply supported bridges under moving vehicle



Phuong Hoa Hoang^{1,*}, Hoang An Thai¹, Dinh Trung Pham²

¹Faculty of Road and Bridge Engineering, The University of Danang–University of Science and Technology, Da Nang, Vietnam

²Department of Civil Engineering, Mien Trung University of Civil Engineering, Tuy Hoa, Vietnam

ARTICLE INFO

Article history:

Received 19 January 2022

Received in revised form

15 April 2022

Accepted 16 April 2022

Keywords:

Approach settlement

Transition slab

Dynamic response

Dynamic foundation

Moving vehicle

ABSTRACT

Reinforced concrete approach slabs serve as a transitional component between the roadway pavement and the bridge deck. Due to the settlement of the embankment soil, the slab is bent, and its slope grade will be suddenly changed resulting in bumps at both ends of the deck; this may increase the dynamic response of bridges induced by the interaction with moving vehicles. In addition, the presence of such bumps not only causes an uncomfortable ride but also exhibits a potentially hazardous condition to the traffic. Since most of the studies have considered either the interaction model between the slab and soil or between the bridge and moving load; in this study, a novel finite element model is established for the bridge under traffic loads, considering the presence of the approach slab that is simulated as a beam rested on a dynamic soil model. The separated models of the approach slab and bridge deck are validated by previous studies and demonstrate their accuracy in predicting the dynamic response of the bridge-vehicle system. A comprehensive parametric study is then performed considering the effect of the soil stiffness, the stiffness of the shear layer of the foundation, and the approach slab length. The results of the study are useful criteria for the practice design of the approach slab in different embankment conditions.

© 2022 The Authors. Published by IASE. This is an open access article under the CC BY-NC-ND license (<http://creativecommons.org/licenses/by-nc-nd/4.0/>).

1. Introduction

The problem of the embankment settlement in the bridge approach is being particularly concern by authorities and designers, which causes unsafety traffics, discomfort for passengers, vehicle damage due to shock loads, and additional effects on the abutment (Ha et al., 2002). The essence of the problem is that the stiffness of the roadway and the bridge deck suddenly changes, resulting in their different settlements. Many approaches have been studied and proposed to control the transient stiffness of these two types of structures, in which an approach slab has been commonly used. This structure enables a smoother transition between the roadway and bridge deck and serves to reduce the dynamic load imposed by heavy trucks on the bridge.

During the service life, the slab may lose its contact with soil due to the embankment settlement,

which can result in vertical faulting to the bridge deck because of the redistribution of load to each end of the slab (Ha et al., 2002; Cai et al., 2005). The presence of vertical faulting between the roadway and the bridge deck may affect the vehicle-induced vibration of the bridge.

In the past decades, many studies have focused on both static and dynamic characteristics of either approach slab or bridge deck subjected to the moving vehicle. Cai et al. (2005) developed a three-dimensional (3D) finite element model (FEM) for the static analysis of the approach slab considering the interaction between the approach slab and the embankment soil. The internal moments in the approach slab due to the dead load and live load were then calculated for different settlement conditions, providing design engineers with a scientific basis to properly design the approach slab. Chen and Fan (2017) developed a simplified bridge approach slab model based on beam-on-elastic Winkler's foundation to investigate the performance of the approach slab. The authors accounted for differential settlements between the approach slab and roadway pavement and soil washouts near the abutment joint. Most recently, Al-Abboodi et al. (2021) investigated the performance of the approach slab under moving vehicles by a 3D dynamic

* Corresponding Author.

Email Address: hphoa@dut.udn.vn (P. H. Hoang)

<https://doi.org/10.21833/ijaas.2022.07.004>

Corresponding author's ORCID profile:

<https://orcid.org/0000-0002-2150-9231>

2313-626X/© 2022 The Authors. Published by IASE.

This is an open access article under the CC BY-NC-ND license

(<http://creativecommons.org/licenses/by-nc-nd/4.0/>)

analysis. In which, the slab is modeled using plate elements while the Mohr-Coulomb material model is adopted for the base, subbase, and subgrade soils. The resulting slab deformations and bending moments provide engineers to understand the response of approach slabs under different conditions of the slab and subgrade.

The uneven approach slab conditions due to the soil settlement is an important factor that affects the vehicle-induced dynamic response of bridges. However, most of the studies often neglect the influence of the bridge approach condition on the bridge-vehicle coupled dynamic response (Deng and Cai, 2010; Gao et al., 2014; Yang and Yang, 2018). One of the few studies was presented by Shi et al. (2008), in which the vehicle-induced dynamic bridge responses are investigated considering the effect of the faulting condition of the approach slab. This faulting condition is considered by different slab deformations at each end and the midspan, and the authors neglect the embankment soil effect. The analysis results show that the faulting condition of the approach slab caused significantly large dynamic responses in the short-span slab bridge.

Based on the above discussions, this study pays attention to a coupled numerical model of the interaction between the bridge and moving load considering the presence of the approach slab. In which, the approach slab rested on the embankment soil is modeled as a beam on a dynamic foundation model, considering the elastic stiffness, stiffness of the shear layer, and mass of the foundation. As a case study, a single span simply supported reinforced

concrete bridge is examined. To simplify the mathematical model, the interaction model of the bridge deck subjected to three moving sprung masses is considered. The examinations of the dynamic response of the bridge deck are performed considering the effects of different embankment soil and approach slab conditions.

In the following, the mathematical model of the bridge deck and approach slab subjected to moving sprung masses is presented in Section 2. Section 3 presents the validation of the numerical model, and a comprehensive parametric study is then performed and discussed. Finally, in Section 4, conclusions along with future perspectives are drawn.

2. Mathematical model

The vehicle-bridge model with the presence of the approach slab is shown in Fig. 1. In which, the bridge and the approach slab can be modeled as two separated systems subjected to moving vehicles. To establish the equation of motion for each system, the following assumptions are used:

- The density, modulus of elasticity, cross-section, and moment of inertia are constant along the beam.
- The speed of the moving vehicle is constant, and the beam is always under the moving load.
- The beam, approach slab, and foundation are linear elastic.

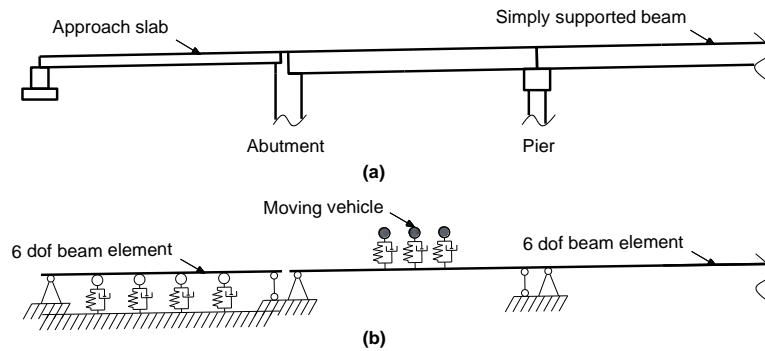


Fig. 1: Vehicle-bridge model with the presence of the approach slab: (a) Schematic of a simply supported beam bridge with approach slab and (b) Numerical model of the bridge subjected to a moving vehicle

The simply supported beam can be modeled using two-dimensional beam elements having 6 degrees of freedom as shown in Fig. 2.



Fig. 2: Beam element model

The axial stiffness matrix of the beam, having elastic modulus E , cross-section A , and element length l , is determined as:

$$K_{bar} = \frac{EA}{l} \times \begin{bmatrix} 1 & 0 & 0 & -1 & 0 & 0 \\ 0 & 0 & 0 & 0 & 0 & 0 \\ 0 & 0 & 0 & 0 & 0 & 0 \\ -1 & 0 & 0 & 1 & 0 & 0 \\ 0 & 0 & 0 & 0 & 0 & 0 \\ 0 & 0 & 0 & 0 & 0 & 0 \end{bmatrix} \quad (1)$$

and the bending stiffness matrix is given as:

$$K_{beam} = \frac{EI}{l^3} \times \begin{bmatrix} 0 & 0 & 0 & 0 & 0 & 0 \\ 0 & 12 & 6l & 0 & -12 & 6l \\ 0 & 6l & 4l^2 & 0 & -6l & 2l^2 \\ 0 & 0 & 0 & 0 & 0 & 0 \\ 0 & -12 & -6l & 0 & 12 & -6l \\ 0 & 6l & 2l^2 & 0 & -6l & 4l^2 \end{bmatrix} \quad (2)$$

The beam stiffness matrix in the global coordinate system is then determined as:

$$K_e = T_e' \times (K_{bar} + K_{beam}) \times T_e, \quad (3)$$

where T_e is the transformation matrix given as:

$$T_e = \begin{bmatrix} \cos \alpha & \sin \alpha & 0 & 0 & 0 & 0 \\ -\sin \alpha & \cos \alpha & 0 & 0 & 0 & 0 \\ 0 & 0 & 1 & 0 & 0 & 0 \\ 0 & 0 & 0 & \cos \alpha & \sin \alpha & 0 \\ 0 & 0 & 0 & -\sin \alpha & \cos \alpha & 0 \\ 0 & 0 & 0 & 0 & 0 & 1 \end{bmatrix}, \quad (4)$$

with α is the inclination angle of the element.

The mass matrix of the beam element in the global coordinate system is,

$$M_e = T_e' \times \rho A l \times \begin{bmatrix} \frac{1}{3} & 0 & 0 & \frac{1}{6} & 0 & 0 \\ 0 & \frac{13}{35} & \frac{11l}{210} & 0 & \frac{9}{70} & \frac{-13l}{420} \\ 0 & \frac{11l}{210} & \frac{l^2}{105} & 0 & \frac{13l}{420} & \frac{-l^2}{140} \\ \frac{1}{6} & 0 & 0 & \frac{1}{3} & 0 & 0 \\ 0 & \frac{9}{70} & \frac{13l}{420} & 0 & \frac{13}{35} & \frac{-11l}{210} \\ 0 & \frac{-13l}{420} & \frac{-l^2}{140} & 0 & \frac{-11l}{210} & \frac{l^2}{105} \end{bmatrix} \times T_e, \quad (5)$$

where ρ is the mass per unit length of the element.

For the approach slab, an Euler-Bernoulli beam rested on a dynamic foundation is modeled (Nguyen et al., 2019). The beam with length L , height h , elastic modulus E , and density ρ is discrete into n elements of length l . Each element has two nodes i and j , and each node has three degrees of freedom including translational and rotational displacements, as shown in Fig. 3.

Using a polynomial shape function matrix $[N]_{w,B}$, the displacement field in the beam element is represented through the nodal displacement vector $\{u\}_{e,B} = \{u_i \ w_i \ \theta_i \ u_j \ w_j \ \theta_j\}^T$, which is represented as:

$$w_{e,B} = [N]_{w,B} \{u\}_{e,B}. \quad (6)$$

The relationship between displacement and deformation of a point in an element is represented by the nodal displacement,

$$\{\varepsilon\}_{e,B} = [B] \{u\}_{e,B}, \quad (7)$$

where $[B]$ is the strain-displacement matrix of the beam element. Then, the stress at a point in the beam element obeys Hooke's law, which is expressed as:

$$\{\sigma\}_{e,B} = [D] \{\varepsilon\}_{e,B} = E[B] \{u\}_{e,B}. \quad (8)$$

The strain energy of the beam element is determined from the bending strain of the beam element and the foundation due to the simultaneous deformation of the elastic foundation layer and the shear layer, determined by,

$$U_{e,B} = \frac{1}{2} \int_{V_e} \varepsilon_{e,B} \sigma_{e,B} dV + \frac{1}{2} \int_0^l k w_{e,B}^2 dx + \frac{1}{2} \int_0^l k_s \left(\frac{\partial w_{e,B}}{\partial x} \right)^2 dx. \quad (9)$$

Substituting Eqs. 6, 7, and 8 into Eq. 9, the strain energy of the beam element is determined by,

$$U_{e,B} = \frac{1}{2} \{u\}_{e,B}^T [K]_{e,B}^b \{u\}_{e,B} + \frac{1}{2} \{u\}_{e,B}^T [K]_{e,B}^w \{u\}_{e,B} + \frac{1}{2} \{u\}_{e,B}^T [K]_{e,B}^s \{u\}_{e,B}. \quad (10)$$

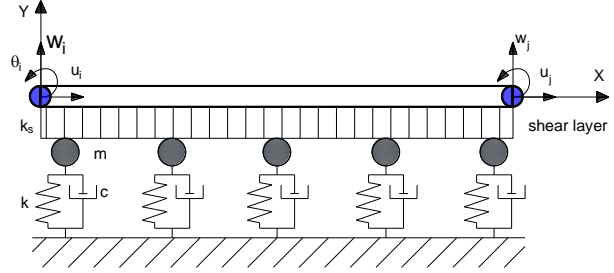


Fig. 3: Beam on dynamic foundation model

Therefore, the stiffness of the beam element on the dynamic foundation includes the stiffness of the beam element under bending, the elastic foundation, and shear layers, given as:

$$[K]_{e,B} = [K]_{e,B}^b + [K]_{e,B}^w + [K]_{e,B}^s, \quad (11)$$

where $[K]_{e,B}^b$, $[K]_{e,B}^w$ and $[K]_{e,B}^s$ are the Euler-Bernoulli beam element stiffness matrix, the foundation layer stiffness matrix, and the shear layer stiffness matrix, respectively, given as:

$$[K]_{e,B}^b = \int_{V_e} [B]^T E [B] dV, \quad (12)$$

$$[K]_{e,B}^w = \int_0^l [N]_{w,B}^T k [N]_{w,B} dx, \quad (13)$$

$$[K]_{e,B}^s = \int_0^l [N]_{s,B}^T k_s [N]_{s,B} dx, \quad (14)$$

where k and k_s are the stiffness of the elastic and shear layers in the dynamic foundation model, and $[N]_s = \partial [N]_B / \partial x$ is the shape function matrix of the rotation angle.

Since displacement is a function of time, the element node velocity also varies with time and is equal to the first derivative of the displacement, which is expressed as:

$$\dot{w}_{e,B} = [N]_B \{\dot{u}\}_{e,B} \quad (15)$$

From that, the kinetic energy of the element is determined by,

$$T_{e,B} = \frac{1}{2} \int_{V_e} \rho \dot{w}_{e,B}^2 dV + \frac{1}{2} \int_0^l m \dot{w}_{e,B}^2 dx. \quad (16)$$

Substitute Eq. 15 into Eq. 16, the kinetic energy of the beam element is given as:

$$T_{e,B} = \frac{1}{2} \{\dot{u}\}_{e,B}^T [M]_{e,B}^b \{\dot{u}\}_{e,B} + \frac{1}{2} \{\dot{u}\}_{e,B}^T [M]_{e,B}^F \{\dot{u}\}_{e,B}. \quad (17)$$

Therefore, the mass matrix of the beam element on the dynamic foundation is determined by,

$$[M]_{e,B} = [M]_{e,B}^b + [M]_{e,B}^F, \quad (18)$$

where $[M]_{e,B}^b$ and $[M]_{e,B}^F$ are the mass matrix of the beam element and the mass matrix of the foundation, respectively, given as:

$$[M]_{e,B}^b = \int_{V_e} [N]_{w,B}^T \rho [N]_{w,B} dV, \quad (19)$$

$$[M]_{e,B}^F = \int_0^l [N]_{w,B}^T m [N]_{w,B} dx. \quad (20)$$

The moving vehicle is modeled as a sprung-mass system, with two nodes associated with two lumped masses of the wheel and the car body, m_w and M_v , respectively. The two masses are connected by the spring and dashpot having the stiffness and damping coefficient denoted by k_v and c_v , respectively (Neves et al., 2012). By assuming the no-jump condition for the moving vehicle, the equation of motion of the vehicle system is given as:

$$\begin{bmatrix} M_v & 0 \\ 0 & m_w \end{bmatrix} \begin{Bmatrix} \ddot{z}_v \\ \ddot{z}_w \end{Bmatrix} + \begin{bmatrix} c_v & -c_v \\ -c_v & c_v \end{bmatrix} \begin{Bmatrix} \dot{z}_v \\ \dot{z}_w \end{Bmatrix} + \begin{bmatrix} k_v & -k \\ -k_v & k_v \end{bmatrix} \begin{Bmatrix} z_v \\ z_w \end{Bmatrix} = \begin{Bmatrix} f_c - (M_v + m_w)g \\ f_c \end{Bmatrix} \quad (21)$$

$$f_c = (M_v + m_w)g + M_v \ddot{z}_v + m_w \ddot{z}_w, \quad (22)$$

where f_c is the contact force, z_v and z_w are the vertical displacements of two nodes, respectively.

Considering the superstructure modeled as beam elements and the approach slab modeled as a beam on the dynamical foundation, which are both subjected to a moving body, the differential equation of motion at the moment $t + \Delta t$ is expressed by,

$$[M]_e \{\ddot{u}_e\}_{t+\Delta t} + [C]_e \{\dot{u}_e\}_{t+\Delta t} + [K]_e \{u_e\}_{t+\Delta t} = \{F\}_{e,t+\Delta t}, \quad (23)$$

where $\{F\}_{e,t+\Delta t}$ is the load vector of the element at time $t + \Delta t$, determined as:

$$\{F\}_{e,t+\Delta t} = -[N]_w f_{c,t+\Delta t} \delta(x_i - vt), \quad (24)$$

where $\delta(x_i - vt)$ is the delta Dirac function; x_i are the coordinates of the moving load; $[M]_e$, $[K]_e$ and

$[C]_e$ are the element mass, stiffness, and damping matrices, respectively.

By assembling the element matrices, a global form of the equation of motion is given as:

$$[M]\{\ddot{U}\} + [C]\{\dot{U}\} + [K]\{U\} = \{F\} \quad (25)$$

where $[M]$, $[C]$, $[K]$ are the global matrix of mass, damping, and stiffness matrices, respectively, and $\{F\}$ and $\{U\}$ are load and nodal displacement vectors of the system. This equation can be solved utilizing the direct step-by-step integration method based on the Newmark algorithm.

3. Numerical analysis

3.1. Description of the case study

The simply supported reinforced concrete bridge in the expressway La Son-Tuy Loan in Central Vietnam is selected as the case study. The bridge is three spans of 1.65 m I beam prestressed reinforced concrete with a span length of 33 m. The cross-section consists of 5 girders spaced 2.4 m, resulting in a total width of the bridge of 12 m. The material and geometry properties of the bridge deck section are shown in Table 1 and the schematic of the bridge cross-section is shown in Fig. 4.

Table 1: Material and geometry properties of the bridge deck section

Quantity	Value	Unit
Area of cross-section	6.193	m ²
Moment of inertial	2.333	m ⁴
Elastic modulus	32980×10 ⁶	N/m ²
Mass density	2450	kg/m ³

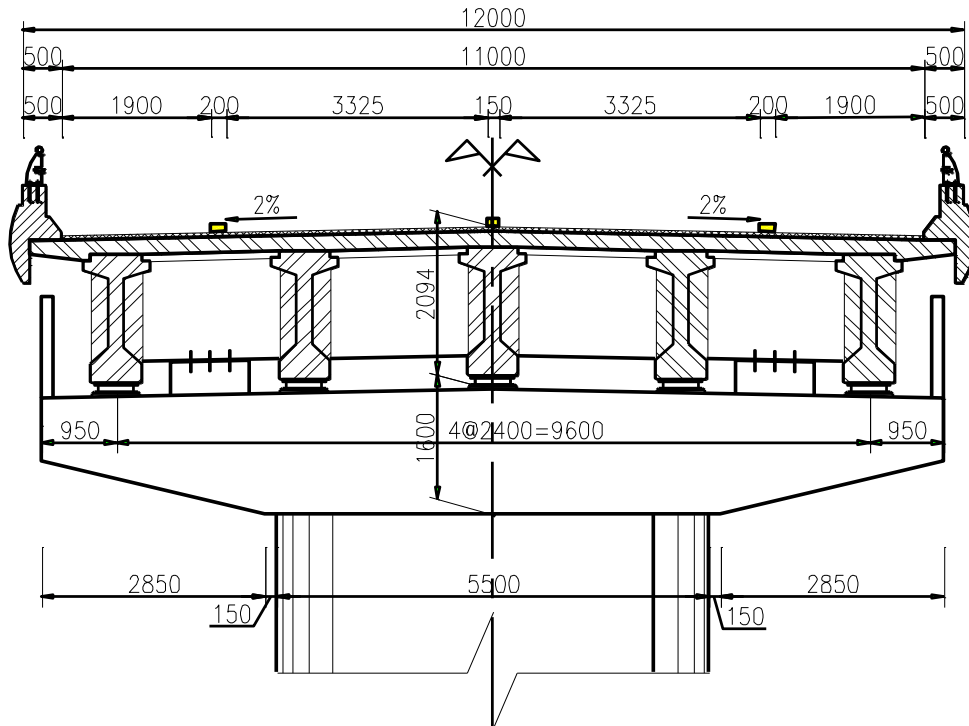


Fig. 4: Schematic of the bridge cross-section

The reinforced concrete approach slab is at each end of the bridge, which serves as a transitional component between the roadway pavement and the bridge deck. The slab, having 0.2 m thickness, 12 m width, and 6 m length, is rested on a compacted embankment with simply supported ends. The soil is assumed to be elastic with an elastic modulus of 100 MPa, a shear layer stiffness of 1×10^7 N/m, and a density of 2000 kg/m³.

3.2. Validation of the numerical model

Due to the lack of literature that considers the coupled model of the approach slab and bridge; in this study, the dynamic responses of the beam on the dynamic foundation and the bridge-vehicle models are separately validated with the available literature.

For the beam on foundation model, the lowest natural frequency is extracted for each case of the dimensionless parameters K_1, K_2 [see Eq. 26, where k is the elastic stiffness, k_s is the stiffness of the shear layer, L is the slab length, and EI is beam section flexural stiffness] of the foundation model and compared with two numerical solutions presented by Matsunaga (1999), in which the damping effect is neglected.

$$K_1 = \frac{kL^4}{EI}, K_2 = \frac{k_s L^2}{\pi^2 EI} \tag{26}$$

The comparison is shown in Table 2 with $K_2 = 1$, the approach slab length and depth ratio $L/h = 10$, and K_1 varied from 0 to 1×10^5 . It can be observed that a very good agreement can be found with the CBT solution and there is a slight difference compared with the TBT solution (Matsunaga, 1999).

Table 2: Validation of the lowest natural frequency of the present beam on the dynamic foundation model

K_1	0	1×10^1	1×10^2	1×10^3	1×10^4	1×10^5
CBT solution Matsunaga (1999)	13.9577	14.3115	17.1703	34.5661	100.9694	316.5356
TBT solution Matsunaga (1999)	13.8162	14.1709	17.0326	34.3963	100.5564	314.9778
Present model	13.9592	14.3129	17.1714	34.5667	100.9697	316.5358

For the bridge-vehicle model, the validation is carried out with the work of Yang et al. (2004). In which, a FEM model was developed for a simply supported beam of length $L = 25$ m subjected to a moving sprung-mass model. The beam is modeled with the cross-sectional area $A = 2$ m², the moment of inertia $I = 0.12$ m⁴, the mass per unit length $m = 4800$ kg/m, and the elastic modulus $E = 27.5$ GN/m². Whereas the vehicle is modeled with the mass $m_v = 1200$ kg, the spring stiffness $k_v = 500$ kN/m, and zero damping; this leads to a bridge mass ratio of 1/100. In the finite element analysis of Yang et al. (2004), 10 beam elements were used for the bridge. The comparison between the two models is shown in Fig. 5 for the vehicle speed $V = 10$ m/s. It can be seen that the present model shows a high degree of coincidence with the previous analytical model (Yang et al., 2004) in terms of the vertical displacement of the midspan. Although very slight deviations exist from the validation, the present numerical models for both the approach slab and bridge are considered acceptable for identifying the key parameters involved.

3.3. Parametric analysis

To examine the effects of embankment soil and slab conditions on the bridge-vehicle response, three cases of the parametric analysis are performed, including the effects of the elastic modulus, the stiffness of the shear layer of the embankment soil, and the approach slab length. The first two parameters of soil are considered the most important factor that affects the dynamic response of the foundation (Deng and Cai, 2010). At each analysis, the impact factor (IM) is calculated as the ratio of the maximum dynamic response and static response. The relationship between $1 + IM$ and different moving speeds for each case is then plotted and discussed. In addition, the vehicle is simplified as three sprung masses, which represent the design truck HL93 defined in AASHTO (2012) with three axles spaced 4.3 m and with axle loads of 35.6 kN and 142.3 kN in the front and the other two, respectively. Table 3 presents the mechanical properties of the sprung-mass models, namely the mass, damping, and stiffness collected from Montenegro et al. (2021) and Hu et al. (2020).

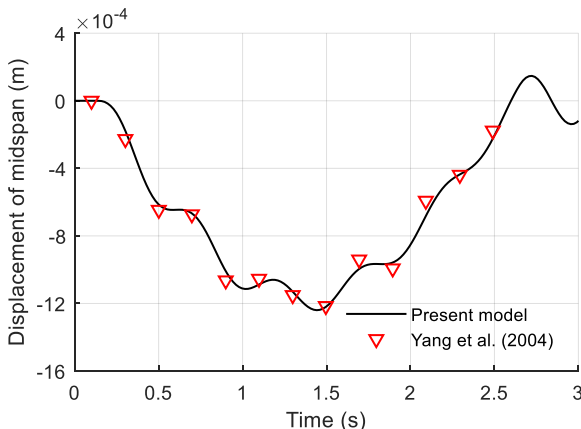


Fig. 5: Validation of the bridge-moving sprung-mass model

Table 3: Parameters of sprung-mass models of the design truck HL93

Quantity	Notation	Value	Unit
Mass of front car body	M_{v1}	2612	kg
Mass of rear car body (equally divided into middle and rear axles)	M_{v2}, M_{v3}	28077/2	kg
Mass of front axle	m_{w1}	490	kg
Mass of middle axle	m_{w2}	808	kg
Mass of rear axle	m_{w3}	653	kg
Damper of the front axle	c_{v1}	2190	N.s/m
Damper of the middle axle	c_{v2}	7882	N.s/m
Damper of the rear axle	c_{v3}	7182	N.s/m
Suspension of the front axle	k_{v1}	242604	N/m
Suspension of the middle axle	k_{v2}	1903172	N/m
Suspension of the rear axle	k_{v3}	1969034	N/m

3.3.1. Influence of elastic stiffness of the foundation

One of the key factors affecting the performance of the approach slab subjected to traffic loads is the condition of the embankment soil (Deng and Cai, 2010; Nguyen et al., 2020). In the first analysis, the effect of the soil stiffness is investigated through the elastic modulus of the soil. In Fig. 6, the time history of the midspan displacement of both the approach slab and bridge deck system is presented. While the dynamic responses of the approach slab for three cases of the elastic modulus, i.e., $E_s = 1, 10, \text{ and } 100 \text{ MPa}$ varies significantly, those of the bridge deck show a similar trend with considerable differences in the peak values. This enables the effect of the presence of the approach slab on the dynamic response of the bridge system.

To investigate in detail the effect of the soil stiffness on the IM factor of the bridge due to the moving vehicle, their relationship for different cases of the vehicle speed is presented in Fig. 7, in which the elastic modulus is varied from 1×10^5 (soft soil) to $1 \times 10^8 \text{ N/m}^2$ (stiff soil), and the horizontal axis is in the logarithmic scale for visualization. In most cases, the $1 + IM$ value decreases with the increase of the soil stiffness. Careful readers can see a considerable decrease in the IM value from $E_s = 1 \times 10^6 \text{ N/m}^2$. And the amplitude of change of the IM value for all the cases varies from 0.026 to 0.038.

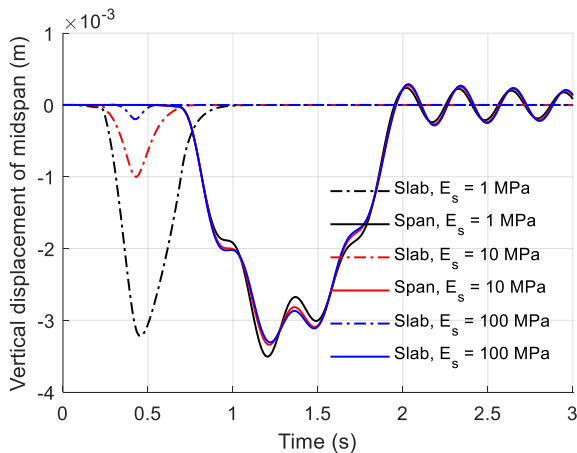


Fig. 6: Time history of the midspan vertical displacement of the approach slab and bridge deck system with different values of the soil elastic modulus

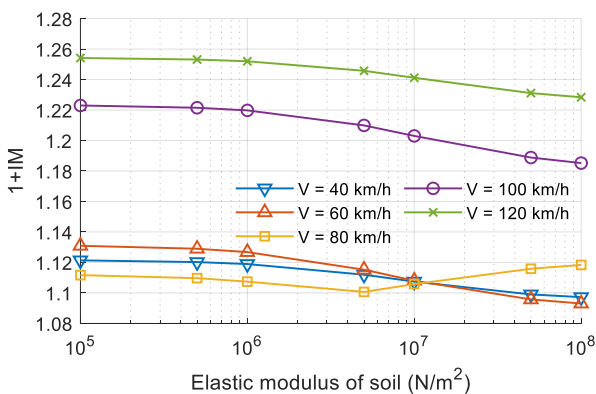


Fig. 7: Variation of IM with the soil elastic modulus

Regarding the vehicle speed, at low speeds, i.e., $V = 40, 60, \text{ and } 80 \text{ km/h}$, the IM values are almost the same concerning the stiffness of the embankment soil. Then, the value of IM increases significantly when the vehicle speeds reach 100 and 120 km/h. The maximum values of $1 + IM$ are 1.223 and 1.254 are recorded at $E_s = 1 \times 10^5 \text{ N/m}^2$ according to $V = 100 \text{ and } 120 \text{ km/h}$, respectively. Those values are smaller than the critical value of $1 + IM$ defined by AASHTO (2012) for this type of bridge, i.e., 1.33. However, it is noticed that a given range of the embankment stiffness is assumed in this study that covers from soft to stiff soil layers. In practice, due to the settlement of the embankment or under deteriorating soil washout conditions, the approach slab may be subjected to large deformations (Cai et al., 2005; Chen and Chai, 2011), thus resulting in large effects on the dynamic response of the bridge deck system.

3.3.2. Influence of shear stiffness of the foundation

In the dynamic foundation model presented in this study, the stiffness of the shear layer is also an important parameter. To investigate the effect of this parameter, different shear stiffness values of the soil are considered, varying from $k_s = 1 \times 10^5$ to $1 \times 10^8 \text{ N/m}$. The time history analysis is first plotted in Fig. 8, and the effects of the soil shear stiffness on the $1 + IM$ value are presented in Fig. 9. Similar observations with the above investigation are recognized. The dynamic response decreases with the increase of the shear stiffness. However, the amplitude of change is rather limited. The peak $1 + IM$ values for five cases of the vehicle speed are 1.121, 1.131, 1.112, 1.211, and 1.247, respectively. Also of note is that at $V = 80 \text{ km/h}$, the dynamic response increases with the increase of the shear layer stiffness; this may be due to the occurrence of the resonance of the vehicle and bridge vibrations at the high shear layer stiffness of the foundation (Museros et al., 2013).

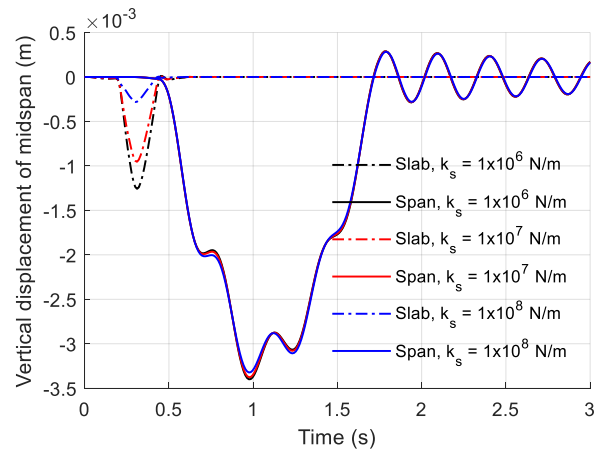


Fig. 8: Time history of the midspan vertical displacement of the approach slab and bridge deck system with different stiffness of the shear layer

3.3.3. Influence of approach slab length

In the practice design of the approach slab, the slab length depends on the height of the abutment and the embankment condition. In this study, the effect of the slab geometry is investigated. Slab lengths from 3 to 12 m are considered (Wang et al., 2014). The time history analysis results for different cases of the slab length are shown in Fig. 10. As seen that the increase of the slab length increases the slab displacement, thus increasing the dynamic response of the bridge.

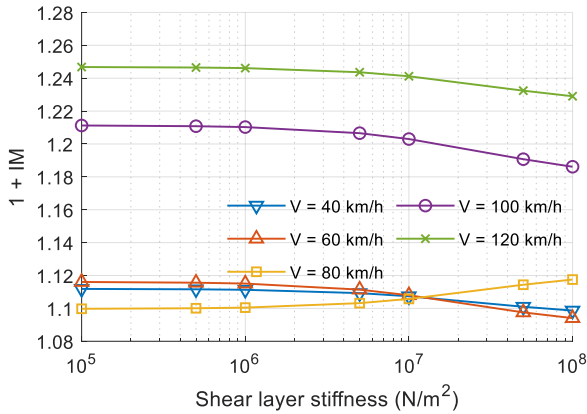


Fig. 9: Variation of IM with the shear layer stiffness

The relationship between the $1 + IM$ value and the approach slab length is shown in Fig. 11. The results are plotted for five cases of vehicle speed. As compared to the above investigations, the trend is different for each case of vehicle speed. While at low speeds, i.e., 40 to 80 km/h, the amplitude of $1 + IM$ is limited (i.e., < 1.12), in the cases of $V = 100$ and 120 km/h, the value of $1 + IM$ is more significant; however, the pattern is different. At $V = 100$ km/h, the $1 + IM$ reaches the peak value corresponding to $L_{slab} = 9$ m, and then the dynamic factor decreases with the increase of the slab until 12 m. On the other hand, the dynamic factor of the bridge increases with the increase of the slab length in the case of $V = 120$ km/h.

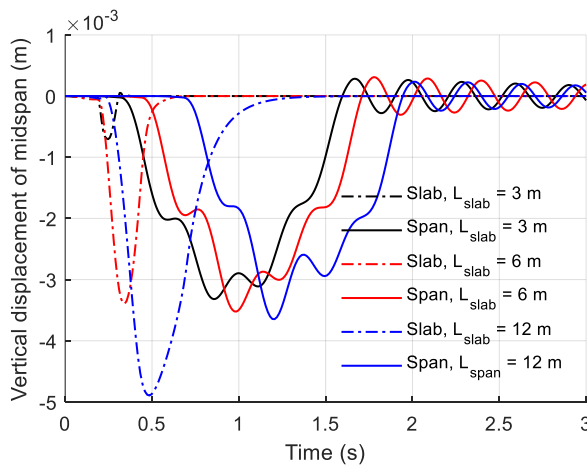


Fig. 10: Time history of the midspan vertical displacement of the approach slab and bridge deck system with different approach lengths

4. Conclusion

This study aimed at presenting a coupled numerical model for the vehicle-bridge interaction with the presence of the approach slab. The FEM was adopted, in which the bridge was modeled using six degrees of freedom beam element, and the approach slab was modeled as a beam rested on a dynamic foundation, considering the effects of elastic stiffness, shear stiffness, and mass of the foundation. The numerical model was validated and agreed well with previous studies.

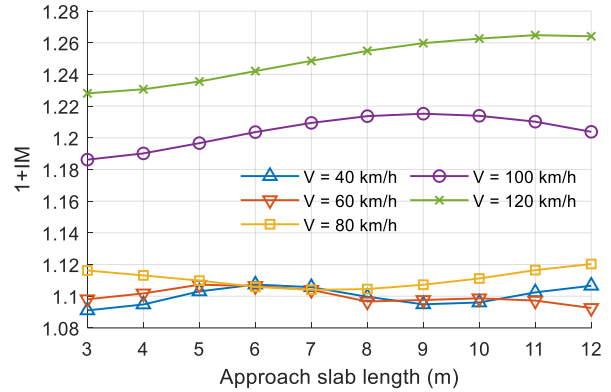


Fig. 11: Variation of IM with the approach slab length

- The parametric study was then performed on a case study of a simply supported prestressed reinforced concrete bridge on the expressway La Son - Tuy Loan in Central Vietnam. The analyses were performed considering the effects of the elastic stiffness of the soil, the stiffness of the shear layer, and the approach length to the dynamic response of the bridge. The results of the parametric study showed significant effects of the examined parameters on the impact factor $1 + IM$ of the bridge, resulting in the following conclusions:
- The decrease of the soil elastic stiffness results in an increase in the dynamic response of the approach slab and the bridge. The amplitude of change is significant in the elastic modulus range from 1×10^6 to 5×10^7 N/m.
- The effect of the shear layer stiffness is the same trend as the above observation; however, the amplitude of change is rather limited and is more significant in the cases of $V = 100$ and 120 km/h.
- The approach length has a significant effect on the dynamic response of the bridge, and the pattern of change is different with the vehicle speeds. Considering all the examined vehicle speeds, approach slab lengths of 6 to 7 m are recommended, in which the $1 + IM$ values for all the cases are in a suitable range. This aspect should be carefully considered in the practice design of the slab.

This study was limited to a case study of the simply supported bridge and the vehicle was simplified to be three sprung-mass models. For further investigation, a more complex vehicle model

should be considered, and the effect of the road roughness should be examined.

List of symbols

A	Element cross-section
E	Element elastic modulus
l	Element length
K_{bar}	Axial stiffness matrix of the beam
K_{beam}	Bending stiffness matrix of the beam
K_e	Stiffness matrix of the beam in the global coordinate system
T_e	Transformation matrix
h	Approach slab height
L	Approach slab length
$[N]_{w,B}$	Polynomial shape function matrix
$\{u\}_{e,B}$	Nodal displacement vector
u_i, u_j	Nodal horizontal displacement
w_i, w_j	Nodal vertical displacement
$w_{e,B}$	Displacement field of a point in the beam element
$[B]$	Strain-displacement matrix
$U_{e,B}$	Strain energy of the beam element
$[K]_{e,B}$	Stiffness of the beam element on the dynamic foundation model
$[K]_{e,B}^b$	Euler-Bernoulli beam element stiffness matrix
$[K]_{e,B}^w$	Foundation layer stiffness matrix
$[K]_{e,B}^s$	Shear layer stiffness matrix
k, k_s	Stiffness of the elastic and shear layers in the foundation model
K_1, K_2	dimensionless parameters of the foundation stiffness
$[M]_{e,B}^b$	Mass matrix of the beam element
$[M]_{e,B}^f$	Mass matrix of the foundation
$[M]_{e,B}$	Mass matrix of the beam element on the dynamic foundation
m_w	Lumped masses of the wheel
M_v	Lumped masses of the car body
c_v	Damping coefficient of the dashpot
k_v	Stiffness of the spring
f_c	Contact force
g	Gravity
$\{F\}_{e,t+\Delta t}$	Load vector
t	Time
Δt	Timestep
z_v, z_w	vertical displacements of two nodes of the vehicle model
α	Longitudinal slope angle of the bridge deck
δ	Delta Dirac function
$\{\varepsilon\}_{e,B}$	Deformation of a point in the beam element
$\{\sigma\}_{e,B}$	Stress at a point in the beam element
ρ	Mass density of the beam

Acknowledgment

This research is funded by Funds for Science and Technology Development of the University of Danang under project number B2019-DN02-55.

Compliance with ethical standards

Conflict of interest

The author(s) declared no potential conflicts of interest with respect to the research, authorship, and/or publication of this article.

References

- AASHTO (2012). AASHTO LRFD bridge design specifications. American Association of State Highway and Transportation Officials, Washington, USA.
- Al-Abboodi I, Al-salih O, and Dakhil A (2021). Dynamic modelling of bridge approach slabs under moving loads. *Journal of King Saud University-Engineering Sciences*, 33(1): 30-36. <https://doi.org/10.1016/j.jksues.2019.12.003>
- Cai CS, Shi XM, Voyiadjis GZ, and Zhang ZJ (2005). Structural performance of bridge approach slabs under given embankment settlement. *Journal of Bridge Engineering*, 10(4): 482-489. [https://doi.org/10.1061/\(ASCE\)1084-0702\(2005\)10:4\(482\)](https://doi.org/10.1061/(ASCE)1084-0702(2005)10:4(482))
- Chen Y and Fan S (2017). Simulation of bridge approach slabs under differential settlement and soil washout. In the World Congress on Advanced in Structural Engineering and Mechanics (ASEM2017), Seoul, Korea: 1-14.
- Chen YT and Chai YH (2011). Experimental study on the performance of approach slabs under deteriorating soil washout conditions. *Journal of Bridge Engineering*, 16(5): 624-632. [https://doi.org/10.1061/\(ASCE\)BE.1943-5592.0000188](https://doi.org/10.1061/(ASCE)BE.1943-5592.0000188)
- Deng L and Cai CS (2010). Development of dynamic impact factor for performance evaluation of existing multi-girder concrete bridges. *Engineering Structures*, 32(1): 21-31. <https://doi.org/10.1016/j.engstruct.2009.08.013>
- Gao Q, Wang Z, Guo B, and Chen C (2014). Dynamic responses of simply supported girder bridges to moving vehicular loads based on mathematical methods. *Mathematical Problems in Engineering*, 2014: 514872. <https://doi.org/10.1155/2014/514872>
- Ha HS, Seo J, and Briaud JL (2002). Investigation of settlement at bridge approach slab expansion joint: Survey and site investigations. Report/Paper Numbers No. FHWA/TX-03/4147-1, Federal Highway Administration, Washington, USA.
- Hu P, Zhang C, Guo W, and Wang Y (2020). Dynamic response of a bridge-embankment transition with emphasis on the coupled train-track-subgrade system. *Applied Sciences*, 10(17): 5982. <https://doi.org/10.3390/app10175982>
- Matsunaga H (1999). Vibration and buckling of deep beam-columns on two-parameter elastic foundations. *Journal of Sound and Vibration*, 228(2): 359-376. <https://doi.org/10.1006/jsvi.1999.2415>
- Montenegro PA, Castro JM, Calçada R, Soares JM, Coelho H, and Pacheco P (2021). Probabilistic numerical evaluation of dynamic load allowance factors in steel modular bridges using a vehicle-bridge interaction model. *Engineering Structures*, 226: 111316. <https://doi.org/10.1016/j.engstruct.2020.111316>
- Museros P, Moliner E, and Martínez-Rodrigo MD (2013). Free vibrations of simply-supported beam bridges under moving loads: Maximum resonance, cancellation and resonant vertical acceleration. *Journal of Sound and Vibration*, 332(2): 326-345. <https://doi.org/10.1016/j.jsv.2012.08.008>
- Neves SGM, Azevedo AFM, and Calçada R (2012). A direct method for analyzing the vertical vehicle-structure interaction. *Engineering Structures*, 34: 414-420. <https://doi.org/10.1016/j.engstruct.2011.10.010>
- Nguyen PT, Pham TD, and Hoang HP (2019). The influence of foundation mass on dynamic response of track-vehicle interaction. *Vietnam Journal of Mechanics*, 41(1): 17-30. <https://doi.org/10.15625/0866-7136/12255>
- Nguyen TP, Pham DT, and Hoang PH (2020). Effects of foundation mass on dynamic responses of beams subjected to moving oscillators. *Journal of Vibroengineering*, 22(2): 280-297. <https://doi.org/10.21595/jve.2019.20729>

Shi X, Cai CS, and Chen S (2008). Vehicle induced dynamic behavior of short-span slab bridges considering effect of approach slab condition. *Journal of Bridge Engineering*, 13(1): 83-92.
[https://doi.org/10.1061/\(ASCE\)1084-0702\(2008\)13:1\(83\)](https://doi.org/10.1061/(ASCE)1084-0702(2008)13:1(83))

Wang ZY, Zhang H, and Wang YJ (2014). Method of determining the length of approach slab for highway bridge. *Advanced Materials Research*, 953: 1657-1662.
<https://doi.org/10.4028/www.scientific.net/AMR.953-954.1657>

Yang YB and Yang JP (2018). State-of-the-art review on modal identification and damage detection of bridges by moving test vehicles. *International Journal of Structural Stability and Dynamics*, 18(02): 1850025.
<https://doi.org/10.1142/S0219455418500256>

Yang YB, Lin CW, and Yau JD (2004). Extracting bridge frequencies from the dynamic response of a passing vehicle. *Journal of Sound and Vibration*, 272(3-5): 471-493.
[https://doi.org/10.1016/S0022-460X\(03\)00378-X](https://doi.org/10.1016/S0022-460X(03)00378-X)